Synthesis, characterization, and optoelectronic properties of phenothiazine-based organic co-poly-ynes

Idris Juma Al-Busaidi,[1] Ashanul Haque,[2]* Rayya Al-Balushi,[3] Jahangir Ahmad Rather,[1] Abdul Munam,[1] Rashid Ilmi,[1] Paul R. Raithby,[4]* Youming Zhang,[5] Yingying Fu,[7] Zhiyuan Xie,[7]* Shuming Chen,[8]* Shahidul M Islam,[9] Wai-Yeung Wong,[5]* Jonathan M. Skelton,[6]* Muhammad S. Khan[1]*

[1] Department of Chemistry, Sultan Qaboos University, P.O. Box 36, Al-Khod 123, Sultanate of Oman.

[2] Department of Chemistry, College of Science, University of Hail, Ha'il 81451, Kingdom of Saudi Arabia.

[3] Department of Basic Sciences, College of Applied Sciences and Health Sciences, A'Sharqiyah University, Ibra 400, Sultanate of Oman.

[4] Department of Chemistry, University of Bath, Bath BA2 7AY, U.K.

[5] Department of Applied Biology and Chemical Technology and Research Institute for Smart Energy, The Hong Kong Polytechnic University, Hung Hom, Kowloon, Hong Kong, P. R. China.

[6] Department of Chemistry, University of Manchester, Oxford Road, Manchester M13 9PL, U.K.

[7] State Key Laboratory of Polymer Physics and Chemistry, Changchun Institute of Applied Chemistry, Chinese Academy of Sciences, Changchun 130022, P. R. China.

[8] Department of Electrical and Electronic Engineering, Southern University of Science and Technology, Shenzhen, 518055, P. R. China.

[9] Department of Chemistry, University of Illinois at Chicago, Chicago, IL 60607.

* Corresponding authors. E-mail: Ashanul Haque: a.haque@uoh.edu.sa (AH)
Paul R. Raithby: p.r.raithby@bath.ac.uk (PRR)
Zhiyuan Xie: xiezy_n@ciac.ac.cn (ZYX)
Shuming Chen: chen.sm@sustc.edu.cn (SMC)
Wai-Yeung Wong: wai-yeung.wong@polyu.edu.hk (WYW)
Jonathan M. Skelton: jonathan.skelton@manchester.ac.uk (J.M.S)
Muhammad S. Khan:msk@squ.edu.om (MSK).

Abstract

We present the synthesis and characterization of seven new organic co-poly-ynes **P1**-**P7** incorporating the phenothiazine (PTZ) motif and evaluate their optoelectronic properties and performance in polymer light-emitting diodes and polymer solar cells (PLEDs/PSCs). The co-poly-ynes were obtained in moderate to high yields *via* Sonogashira coupling reactions and characterized using analytical, spectroscopic and electrochemical techniques and complementary quantum-chemical modelling. The materials show strong optical absorption in the visible region of the spectrum and most also show strong emission with quantum yields in the range of 13-41 % relative to Rhodamine 6G (R6G). PLED devices based on the co-poly-ynes were prepared and the most promising was measured to have a brightness of up to 1.10×10^4 cd m^{-2}. PSCs based on donor materials incorporating some of the polymers were prepared and demonstrated power conversion efficiencies of up to 0.24 %.

Keywords: Phenothiazine (PTZ); co-poly-ynes; optoelectronic properties, electrochemical properties; polymer light emitting diodes (PLEDs); polymer solar cells (PSCs)

1. Introduction

Conjugated polymers are an important class of materials used in many real-world applications.[1, 2] Among a plethora of small, medium and large conjugated molecular systems, co-poly-ynes containing alkynyl functionality in the main chain have attracted significant contemporary research interest due to the physical properties imparted by the alkynyl units. These include, for example, a linear geometry, structural rigidity, extended π-electron delocalization, and dual-emission behavior, among others. In the past, we have reported several organic and organometallic poly-ynes for opto-electronic applications,[2, 3] and one of us has demonstrated the photovoltaic (PV) effect in a poly(platina-yne).[4] Since then, several researchers have investigated the PV properties and performance of small, medium and large conjugated poly-ynes, and solar cells based on this class of materials have been reported.[1, 2] Both the alkynyl units and the nature of the spacer groups play a pivotal role in defining the properties of poly-yne materials,[5, 6] and both electron-rich and electron-deficient carbocyclic and heterocyclic spacers have been investigated for PV applications.[7, 8]

Among several known heterocyclic spacers, phenothiazine (PTZ), a tricyclic electron-rich chromophore containing nitrogen and sulfur heteroatoms, has intriguing electrochemical and photo-physical properties.[9, 10] One of us reported several dye-sensitized solar cells (DSSCs) and bulk-heterojunction PV (BHJ-PV) cells based on the PTZ core.[11-15] The DSSC performance of Pt(II) di-ynes incorporating the PTZ moiety was found to be close to the N719 standard.[15] The PTZ moiety provides a rigid planar biphenyl unit within the polymer backbone and can be readily functionalized at the N heteroatom, providing routes to improve the processability, to facilitate inter-chain interactions in films, and to enhance the charge separation.[11, 12] The presence of electron-rich nitrogen and sulfur heteroatoms in a heterocyclic structure imparts PTZ with a strong electron-donating ability, and its non-planar butterfly conformation can inhibit molecular aggregation and excimer formation, potentially enhancing the performance of PV devices.[16, 17]

While several studies have investigated dyads and triads as PV materials,[18] there are presently no reports of co-poly-ynes incorporating PTZ as an electron-donor fragment. Motivated by the unique properties of PTZ and the absence of studies on organic poly-ynes incorporating this moiety, we have designed and synthesized seven new PTZ-based organic co-poly-ynes (**P1**-**P7**). In order to achieve low-band gap materials, we have judiciously incorporated fused and non-fused heterocyclic spacer units including thiophene, 2,2'-bithiophene and thieno[3,2-b]thiophene alongside PTZ within the polymer backbone.

In this work, we present a comprehensive characterization of the optoelectronic and electrochemical properties of the seven co-poly-ynes, including quantum-chemical modelling using density-functional theory, and we assess their performance in polymer light-emitting diode (PLED) and polymer solar cell (PSC) devices.

2. Results and discussion

2.1. Synthesis and spectroscopic characterization

The PTZ-based alkynyl ligand 10-(2-ethylhexyl)-3,7-diethynyl-10*H*-phenothiazine (**1**) was prepared in quantitative yield by reacting phenothiazine with 2-ethylhexyl bromide and ^{t}BuOK in THF according to previously reported procedures[19] (**Scheme 1**). The alkylated PTZ (**1**) was then brominated with N-bromosuccinimide (NBS) to obtain 3,7-dibromo-10-(2-ethylhexyl)-10*H*-phenothiazine (**2**) according to an adapted literature method.[20] The protected ligand precursor 3,7-bis(trimethylsilylethynyl)-*N*-(2-ethylhexyl) 10H-phenothiazine (**3**) was obtained by the Pd(II)/Cu(I)-catalyzed cross-coupling of the dibromo-PTZ species (**2**) and trimethylsilylethynyl (TMSE) in $^{i}Pr_2NH$/THF. The resulting product was deprotected using aqueous KOH in MeOH/THF and purified using silica gel column chromatography, giving 10-(2-ethylhexyl)-3,7-diethynyl-10*H*-phenothiazine (**4**) as a light-yellow viscous liquid in 95 % yield. Sonogashira cross-coupling reactions between (**4**) and a range of dibromo aromatic spacers (Br-Ar-Br) in a 1:1 ratio produced the organic co-poly-ynes **P1**-**P7** in good to moderate yields of 28-83 %, which were subsequently purified by silica gel column chromatography followed by precipitation in CH_2Cl_2/methanol.

The seven co-poly-ynes were characterized by IR and ^{1}H and ^{13}C NMR spectrsoscopies. The IR spectra confirmed the presence of the C≡C bonds from the characteristic peaks around 2079-2210 cm^{-1}. The ^{1}H and ^{13}C NMR spectra of the compounds showed the expected peaks corresponding to the alkyl, aryl and alkynyl fragments. Polystyrene-equivalent molecular weights (M_n, M_w) and polydispersity indices (PDI = M_w/M_n) were determined by gel permeation chromatography (GPC) using a linear polystyrene standard calibration curve. GPC provides absolute molecular weights for all of the co-poly-ynes part from **P3** and **P4**, for which the comparatively low molecular weights and the sensitivity of the multi-angle laser light scattering detector meant we could only obtain apparent molecular weights. These measurements give weight-average molecular weights in the range of (4,000-50,000 g mol^{-1}), corresponding to weight-average degrees of polymerization (X_w) between 13 and 213 (**Table 1**). The synthesized co-poly-ynes were found to have relatively narrow molecular weight distributions with PDIs between 1.12-1.78. These molecular weights should however be viewed with caution in view of the difficulties of using GPC to characterize rigid-rod polymers.

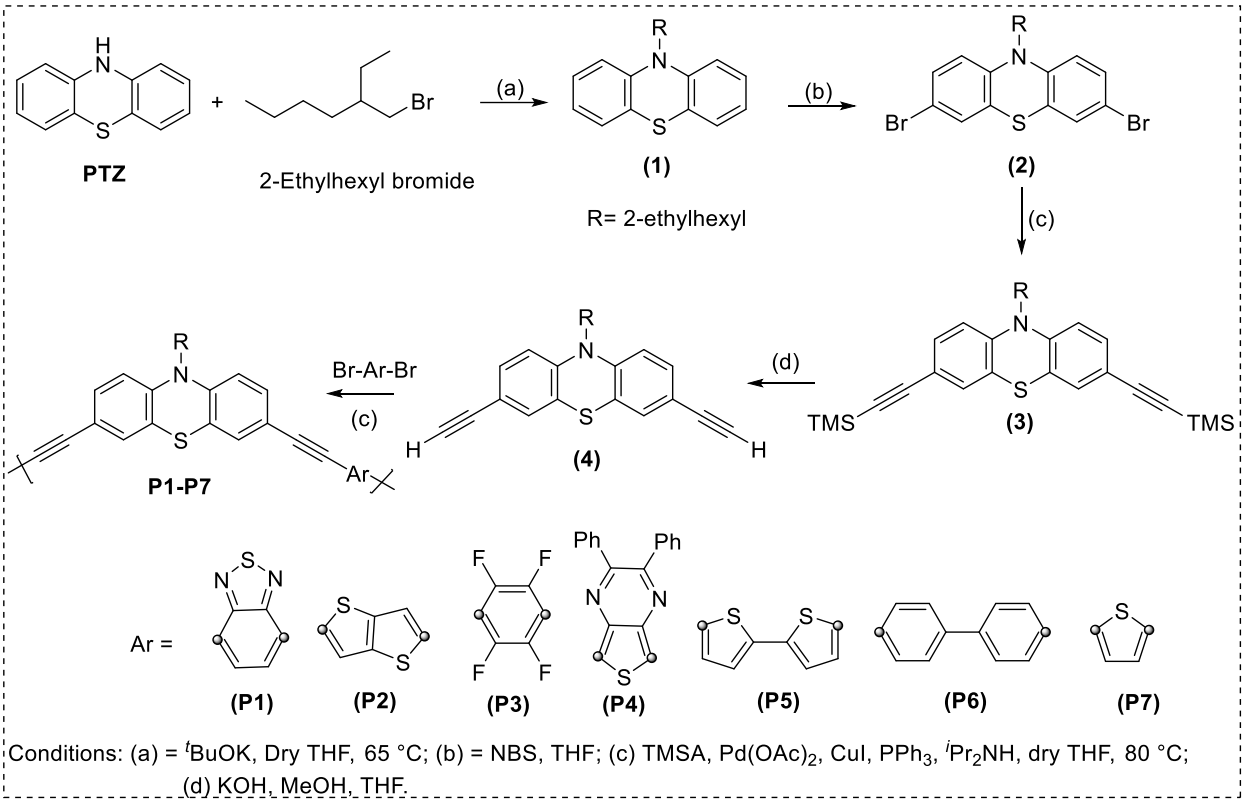

Scheme 1 Preparation of the organic co-poly-ynes **P1**-**P7**.

Table 1 Weight- and number-average molecular weights M_w/M_n, polydispersity indices (PDIs) and degrees of polymerization X_w/X_n for the synthesized co-poly-ynes **P1**-**P7**.

	M_w (g mol^{-1})	M_n	PDI	X_w	X_n
P1	50,100	44,600	1.12	213	190
P2	6,000	4,500	1.35	26	19
P3	4,200	2,400	1.78	18	10
P4	3,950	2,300	1.73	13	7
P5	16,900	13,800	1.22	68	55
P6	20,700	13,600	1.53	85	56
P7	6,000	4,650	1.29	29	22

2.2. Photophysical properties

The room-temperature optical absorption and emission spectra of **P1**-**P7** were measured in 10^{-5} M CH_2Cl_2 solution and the results are given in **Figures 1/2** and **Table 2.**

The absorption spectra of all seven polymers exhibit two absorption bands between 225-325 nm and 360-550 nm (**Figure 1**). The former can be assigned to π→π* electronic transitions on the chromophores (Soret bands) while the latter can be attributed to intra-molecular charge transfer (ICT) from the donor to the acceptor moieties (Q bands).[21] The measurements clearly highlight the sensitivity of the ICT band to the organic spacers. When an alkynyl linker is connected to a strong electron-donating moiety such as PTZ it acts as an electron acceptor, giving rise to donor-acceptor (D-A) interactions, and these can be reinforced

by connecting an electron-accepting moiety to the PTZ *via* the alkynyl linker. It has been shown that the D-A interactions are more prominent in organic polymers than in related metallopolymers.[22]

The trends in the absorption profiles can be understood by considering the electron withdrawing nature and conjugation length of the acceptor spacers connected to the donor PTZ. It is well established that fluorinated aryl, 2,1,3-benzothiadiazole, and 2,3-diphenylthieno[3,4-b]pyrazine have strong electron-withdrawing ability[23-25] and their electron-accepting strength varies in the order of tetrafluoro phenylene < 2,1,3-benzothiadiazole < 2,3-diphenylthieno[3,4-*b*]pyrazine. We found the same trend in the present systems, with the optical band gap ($E_{\mathrm{g,opt}}$) of the co-poly-ynes increasing in the order of **P4** (1.92 eV) < **P1** (2.15 eV) < **P3** (2.57 eV). **P2**, **P5** and **P7** all have S-containing five-membered heterocyclic spacers but exhibit different $E_{\mathrm{g,opt}}$ due to differences in conjugation length. One of us has previously demonstrated that fused thiophenes are less conjugated while bithiophenes are more so due to different numbers of C=C bonds.[26] The same holds true for the PTZ polymers reported in this work, with the $E_{\mathrm{g,opt}}$ falling in the order **P5** (2.51 eV) < **P7** (2.60 eV) ~ **P2** (2.63 eV). Comparing both sets of co-poly-ynes, we conclude that the 2,1,3-benzothiadiazole and thieno[3,2-*b*]thiophene spacers induce the strongest D-A interactions when connected to PTZ, followed by the tetrafluorophenyl and S-based heterocycles.[27]

Table 2 Optical absorption maxima, optical bandgaps $E_{\mathrm{g,opt}}$, and emission maxima, quantum yields and Stokes shifts of the co-poly-ynes **P1**-**P7**. All measurements were performed at room temperature in 10^{-5} M CH_2Cl_2 solution. Quantum yields are were measured relative to Rhodamine 6G (R6G).

	Absorption		**Emission**			
	λ (nm) ($\varepsilon \times 10^4$ mol^{-1} cm^{-1})	**Optical band gap $E_{\mathrm{g,opt}}$ (eV)**	**λ_{ex} (nm)**	**λ_{em} (nm)**	**ϕ_F (%)**	**Stokes shift (cm^{-1})**
P1	487 (10.0), 354 (8.2), 316 (15.2), 255 (13.5)	2.15	-	N/A[a]	-	-
P2	420 (4.9), 324 (4.4), 299 (6.6), 230(14.0)	2.63	420	512	29.0	4278
P3	425(10.3), 304(7.9), 237(8.1)	2.57	416	556	17.0	5544
P4	545 (10.6), 379 (18.1) 335 (22.9), 279 (21.0)	1.92	-	N/A[a]	-	-
P5	429 (13.8), 356 (8.4), 288 (8.4), 238(8.3)	2.51	418	534	14.0	4583
P6	416 (5.8), 319 (6.8), 298 (9.3), 229(7.6)	2.62	408	509	41.0	4392
P7	419 (10.2), 327 (10.0), 291 (8.4), 236 (7.7)	2.60	407	520	13.0	4635

[a]**P1** and **P4** did not show detectable emission at room temperature.

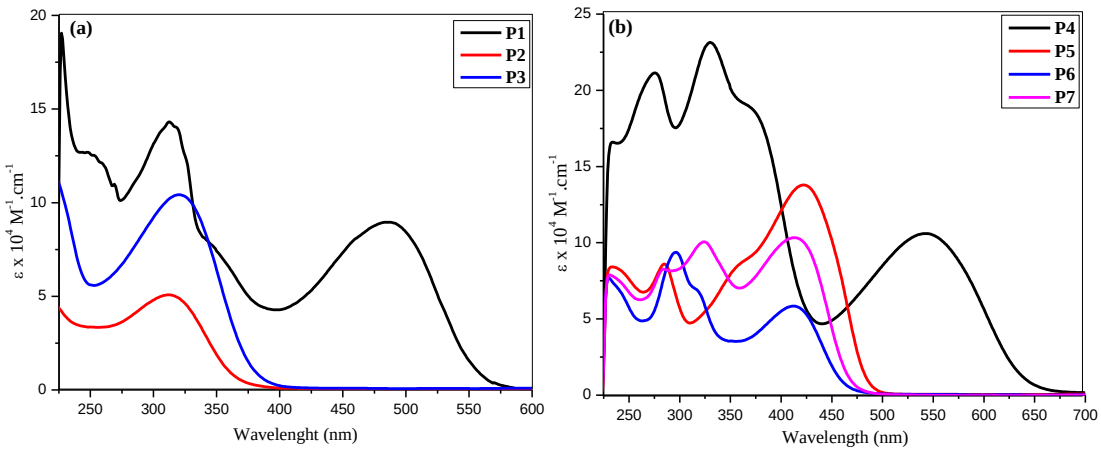

Figure 1 Room temperature optical absorption spectra of the organic co-poly-ynes (a) **P1** – **P3** and (b) **P4 – P7** measured in 10^{-5} M CH_2Cl_2 solution.

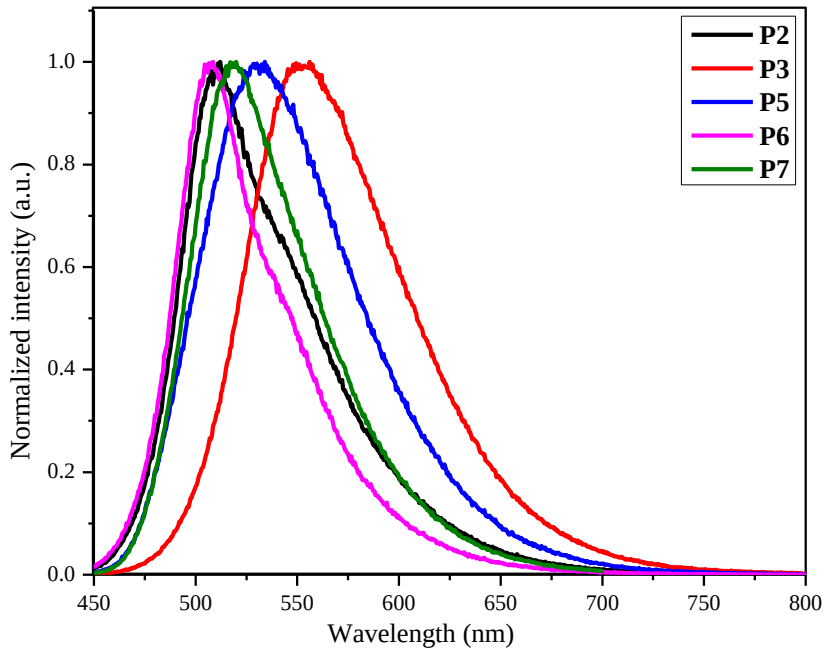

Figure 2 Room temperature fluorescence emission spectra of the organic co-poly-ynes **P2**, **P3**, **P5** – **P7** in 10^{-5} M CH_2Cl_2 solution collected at the excitation wavelengths listed in **Table 2**.

Figure 2 compares the room-temperature emission spectra of the organic co-poly-ynes. With the exception of **P1** and **P4**, the co-poly-ynes show a single florescence band between 450-600 nm which we assigned to the S_1 singlet excited state. Large Stokes shifts of 4278-5544 cm^{-1} (**Table 2**) can be attributed to structural changes occurring in this state, with the bent ground-state structure becoming more planar in on the S_1 potential-energy surface.[28] The nature of the acceptor spacer group can be seen to have a substantial impact on the emission profile, with the emission maxima (λ_{em}) varying in the order **P3** > **P5** > **P7** > **P2** > **P6**. As for the absorption spectra, the emission spectrum of **P6** was found to be the most blue-

shifted, which could be attributed to the biphenyl moieties adopting a more twisted conformation. The quantum yields ϕ_F of the polymers determined relative to the rhodamine 6G dye (R6G; **Table 2**) highlight the crucial role of the extent of the conjugation, with **P6** and **P7** having the highest and lowest values of ϕ_F = 41 and 13 % respectively.

2.3. Computational modelling

To better understand the optical spectroscopy, we performed quantum-chemical calculations using hybrid density-functional theory (DFT) on the precursor PTZ moiety **4** and a set of model compounds **M1**-**M7** approximating **P1**-**P7**. **M1**-**M7** each comprise a chain of three PTZ and two spacer moieties, with the terminal alkyne groups capped by methyl substituents. Images and coordinates of the optimized structures of **4** and **M1**-**M7** can be found in **Figures S1**-**S8** and **Listings S1**-**S8** (Supporting Information).

Table 3 Calculated frontier highest-occupied and lowest-unoccupied orbital (HOMO/LUMO) energies and bandgaps of the precursor PTZ moiety **4** and the model compounds **M1**-**M7**. The orbital energies are expressed as a difference in energy $\Delta E_{\mathrm{HOMO}}/\Delta E_{\mathrm{LUMO}}$ relative to **4**.

	ΔE_{HOMO} [Ha]	ΔE_{LUMO} [Ha]	E_{g} (eV)
4	0	0	6.25
M1	0.285	-1.588	4.38
M2	0.319	-0.934	5.00
M3	0.132	-1.105	5.01
M4	0.489	-1.583	4.18
M5	0.326	-0.966	4.96
M6	0.229	-0.651	5.37
M7	0.355	-0.809	5.09

The calculated HOMO-LUMO bandgaps E_{g} are shown in **Table 3**, and isosurface plots of the frontier orbitals are shown in **Figures S9**-**S16** (Supporting Information). Qualitatively, the bandgaps fall into a rough grouping of **4** > **M2**, **M3**, **M5**, **M6**, **M7** > **M1**, **M4**, where **4** has the widest E_{g} of 6.25 eV, five of the model compounds have bandgaps in the range of 4.96-5.37 eV, and **M1** and **M4** have the narrowest E_{g} of 4.38 and 4.18 eV respectively. The bandgaps in the model compounds are thus reduced by 16-33 % relative to the PTZ precursor **4**. Inspection of the frontier orbitals shows that **M1**-**M7** have heavily delocalized HOMOs that extend across all three PTZ moieties and both spacer groups. On the other hand, the LUMOs, while also very delocalized, do not extend completely across the two terminal PTZ units. Interestingly, the nodal pattern in the HOMO and LUMO of **4** are reflected in the corresponding frontier orbitals of the model compounds, which may be taken to suggest that the frontier orbitals of the model compounds consist, to first approximation, of combinations of the frontier orbitals on the subunits.

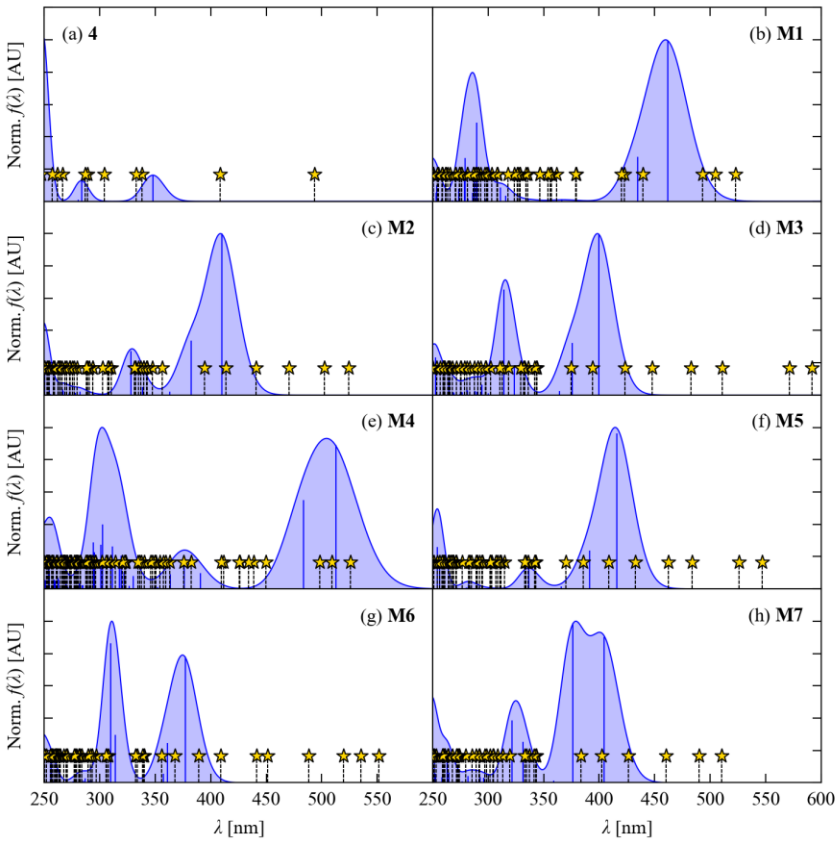

Figure 3 Simulated absorption spectra of the precursor PTZ moiety **4** (a) and the model compounds **M1**-**M7** (b)-(h), obtained from TD-DFT calculations. The spectra shown as shaded blue curves were calculated based on the energies and dipole oscillator strengths of the spin-allowed (singlet) transitions and a nominal Gaussian broadening with a width σ = 0.1 eV. The positions and relative intensities of the individual transitions are marked with vertical blue lines. The energies of spin-forbidden (triplet) states are marked as dashed lines with gold stars.

Taking the orbital energies of **4** as a reference point, we find that the HOMOs of the model compounds are raised in energy (i.e. destabilized) by 0.1-0.5 eV while the LUMOs are lowered in energy (i.e. stabilized) by 0.6-1.6 eV. While both will ultimately have an effect on narrowing the bandgap, these numbers suggest that the stabilization of the LUMO in the model compounds has the largest impact on the bandgap. Indeed, the LUMOs of **M1** and **M4** are calculated to be ~0.5 eV lower in energy than any of the other model compounds relative to **4**, which goes some way to accounting for the narrower bandgaps of these two systems.

The calculated bandgaps are 1.9-2.2 × larger than the measured optical bandgaps in **Table 2** and are also larger than the electrochemical bandgaps presented in the following section (see **Table 7**). Furthermore, they are also considerably larger than the lowest-energy singlet (spin-allowed) optical excitations predicted from time-dependent DFT (TD-DFT) calculations (**Table 4**). This discrepancy may be

ascribed to fundamental limitations of ground-state Kohn-Sham DFT,[29] and/or to the truncated model compounds being an approximation to the extended electronic structure of the polymers. The E_g nevertheless correctly predict that **P1** and **P4** have the lowest $E_{g,opt}$ while the other systems fall into a similar range, and the 1.2 eV range between **M1**-**M7** is proportionally larger than the 0.71 range between the measured $E_{g,opt}$ of **P1**-**P7**.

Simulated absorption spectra (**Figure 3**) reproduce the main qualitative trends in the measured spectra in **Figure 1**, and, in particular, correctly predict the longer-wavelength absorption maxima in **P1** and **P4** and the similar positions of the maxima in the spectra of the other five co-poly-ynes. The simulated spectrum of **M7** (**Figure 3h**) predicts a split long-wavelength band comprised of two almost equally intense transitions - while this splitting is not clearly visible in the measured spectrum of **P7** in **Figure 1**, the absorption maximum does have an asymmetric band shape, and the discrepancy may therefore be due simply to our choice of broadening. Quantitatively the absorption maxima are blue shifted by 10-40 nm relative to the measurements, which may be ascribed to solution effects and/or the extended conjugation in the co-poly-ynes compared to the model compounds. While the former could be tested and corrected by performing the calculations using an implicit-solvent model, we opted not to do this in the present calculations as we doubt that a single solvent environment would capture the range of environments in the solution measurements and test devices investigated in this work.

Table 4 Characterization of the brightest spin-allowed (singlet) transitions in the precursor PTZ moiety **4** and the model compounds **M1**-**M7**. The states are labelled such that S_0 is the ground state and S_1 and S_2 the first and second excited states respectively. For each state, the energy and wavelength are given in eV and nm together with the dipole oscillator strength *f*.

	State	*E* (eV)	*λ* (nm)	*f*
4	S_1	3.56	348	0.135
M1	S_1	2.68	462	2.712
M2	S_1	3.03	410	3.681
M3	S_1	3.10	400	2.747
M4	S_1	2.42	513	1.660
	S_2	2.56	484	1.022
M5	S_1	2.98	416	4.161
M6	S_1	3.29	377	2.599
M7	S_1	3.06	405	1.772
	S_2	3.29	376	1.941

Table 4 lists the brightest 1-2 spin-allowed (singlet) transitions giving rise to the longest-wavelength absorption peaks in each of the simulated spectra. A breakdown of each of the transitions listed in **Table 4** into component transitions between pairs of occupied and virtual states is given in **Tables S1**-**S10** (Supporting Information). This data clearly shows that the transitions in the model compounds are significantly red shifted compared to **4** and show a 5-30 × enhancement in the dipole oscillator strengths. The S_1 state in **4** can be assigned as a "pure" HOMO → LUMO transition. With the exception of the S_2 states in **M4** and **M7**, the HOMO → LUMO transition is the largest component of the brightest transitions in

the model compounds, but only accounts for ~45-60 % of the electron-density redistribution on the sum of squared coefficients. In the S_2 state of **M4**, the HOMO → LUMO + 1 and HOMO - 1 → LUMO account for 51 and 34 % of the sum of squared coefficients, respectively. In the S_2 state of **M7**, the dominant components are again the HOMO → LUMO + 1 and HOMO - 1 → LUMO transitions, which account for 38 and 32 % of the sum of squared coefficients.

To further investigate the nature of the transitions, we used the method of natural transition orbitals (NTOs)[30] to visualize the occupied particle and virtual hole states associated with each of the transitions listed in **Table 4** (**Figures S17**-**S26**). For the precursor PTZ moiety **4**, the NTO analysis yields a single pair or NTOs corresponding to the HOMO and LUMO and the S_1 state can be assigned as a $\pi \rightarrow \pi^*$ transition. For the model compounds, the NTO analysis yields two pairs of NTOs with > 10 % contribution to the transition. In most cases, both NTOs closely resemble the delocalized HOMOs and LUMOs, albeit with reduced contributions from the terminal PTZ units. The NTO analyses therefore show that that the transitions involve a redistribution of the electron density across large parts of the molecules, but it is difficult to assign them definitively as ICT or $\pi \rightarrow \pi^*$. Two notable exceptions to this pattern are the S_1 state in **M5**, for which the electron density in the largest contributing transition is concentrated around the central PTZ moiety, and the S_2 state in **M7**, which consists of two component transitions between states partly localized on the two halves of the molecule.

Extrapolating from the model compounds to the polymers, one might anticipate that the extended structure would produce a large number of states that are closely spaced in energy (i.e. a “bandwidth”), which would in turn produce a high density of optically-bright transitions. This supports the hypothesis that, by tuning the bandgap through suitable selection of the spacer group, it should be possible to engineer co-poly-ynes with strong visible absorption, as we demonstrate in this work.

Table 5 Energies and wavelengths of the lowest-lying spin-forbidden (triplet) transition T_1 in each of the precursor PTZ moiety **4** and the model compounds **M1**-**M7**.

	E **(eV)**	***λ*** **(nm)**
4	2.51	494
M1	1.41	882
M2	1.83	676
M3	2.09	592
M4	1.03	1206
M5	1.74	712
M6	2.25	551
M7	1.88	659

Finally, we note that the simulated spectra in **Figure 3** indicate the presence of spin-forbidden (triplet) states. The energies and wavelengths of the lowest-lying T_1 states are collected in **Table 4**. The T_1 states invariably have lower energies than the S_1 states, and for some of the model compounds even extend into the infrared part of the spectrum. However, given their nature, it is not clear how accessible these states

would be and therefore what role they would play in the optical properties. Discerning this would require further, somewhat involved, excited-state calculations that are beyond the scope of this study.

2.4. Electrochemical properties

To investigate the electro-catalytic properties of the co-poly-ynes, polymer-modified interfaces were fabricated by drop casting 5 µL of 1.0 mg L^{-1} stock THF solutions of each of the polymers onto glassy carbon electrodes (GCEs).

Electrochemical impedance spectroscopy (EIS) was performed to examine the electro-catalytic properties of the modified interfaces in aqueous solutions of 1 mol L^{-1} KNO_3 containing 10^{-2} mol L^{-1} of the $[Fe(CN)_6]^{3-/4-}$ redox system (**Figure 4**). The Randles equivalent circuit used to fit the spectra (**Figure 4**, inset) consists of four components, where C_{dl} is the double-layer capacitance of the system, R_{ct} is the charge-transfer resistance, Z_w is the Warburg impedance, and R_s is the resistance of the electrolyte.[31]

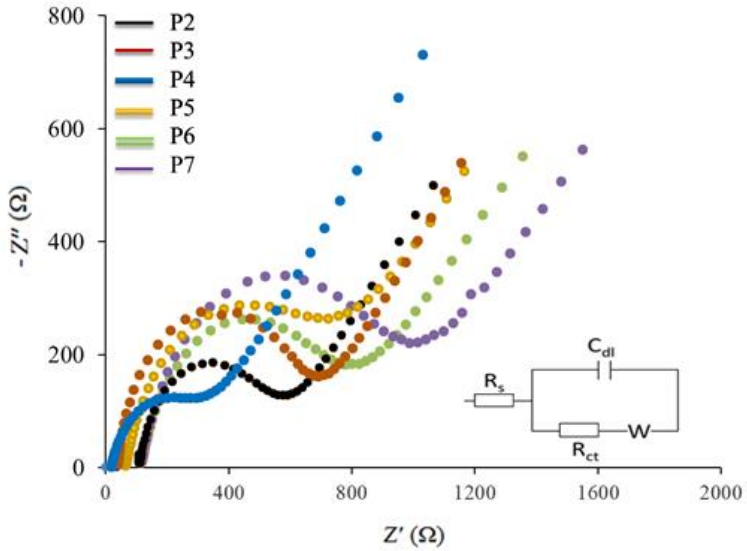

Figure 4 Electrochemical impedance spectra of polymer-modified interfaces with **P2**-**P7** in aqueous solutions containing 1 mol L^{-1} KNO_3 and 10^{-2} mol L^{-1} of the $[Fe(CN)_6]^{3-/4-}$ redox system. As noted in the text, **P1** showed no electrocatalytic activity in these measurements.

R_{ct} is determined by analysis of the Nyquist plots and represents the rate of electron transfer to and from the redox probe at the electrode-solution interface. Among the modified interfaces, the **P4** interface shows the lowest charge-transfer resistance (R_{ct} = 652 Ω), which can be attributed to the efficient delocalization of π-electrons between the PTZ donor and 2,3-diphenylthieno[3,4-b]pyrazine acceptor unit *via* the alkynyl linkage. Inspection of the charge-transfer resistances of the other modified interfaces reveals that the electron-transfer kinetics follows the order of **P5** (R_{ct} = 725 Ω) > **P3** (R_{ct} = 850 Ω) > **P2** (R_{ct} = 925 Ω) > **P6** (R_{ct} = 980 Ω) > **P7** (R_{ct} = 1210 Ω). **P1** showed no electrocatalytic activity in our EIS measurements, which we attributed to the electrode surface being blocked by the co-poly-yne.

Based on these results, the following conclusions can be drawn: (a) **P2**, containing the fused thiophene, is less conjugated than its bithiophene counterpart **P5**; (b) the presence of the electronegative fluorine atoms in **P3** creates a pull, leading to faster electron-transfer kinetics;[32] and (c) there is a smaller D-A interaction in polymers containing just biphenyl and thiophene (**P6**/**P7**). These results are in line with the photophysical measurements and computational modelling, and further highlight the importance of the spacer group in determining the physical properties.

The modified interfaces were further examined by cyclic voltammetry (CV) measurements using the same $[Fe(CN)_6]^{3-/4-}$ redox probe. **Figure 5** shows the voltammograms obtained by scanning the potential between -0.2 and 0.6 V at 50 mV s^{-1}. The modified interfaces show well-defined quasi-reversible redox peaks with a satisfactory redox peak separation and high current response facilitating the charge transfer kinetics (**Figure 5**, **Table 6**). Again, **P1** showed no electrocatalytic activity.

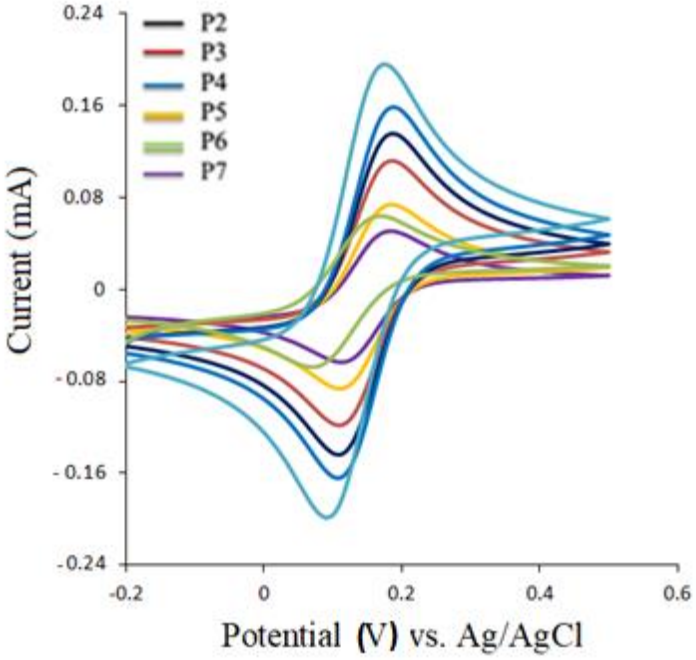

Figure 5 Cyclic voltammograms of polymer-modified interfaces with **P2** – **P7** in 10^{-2} mol L^{-1} aqueous solutions of $[Fe(CN)6]^{3-/4-}$ with 1 mol L^{-1} KNO_3.

A further set of CV measurements were performed on the polymer-modified interfaces in 0.1 M Bu_4NPF_6/CH_2Cl_2 solution using ferrocene as a reference to determine the redox potentials of the co-poly-ynes. All seven co-poly-ynes exhibited quasi-reversible oxidation and reduction (**Figure 6**, **Table 7**). The multiple pseudo-reversible oxidations observed for the co-poly-ynes are similar to other reports on oligomers,[33] co-polymers[34] and homopolymers[35] of PTZ.

Table 6 Electrochemical properties of polymer-modified interfaces with **P2**-**P7** in 10^{-2} mol L^{-1} aqueous solutions of $[Fe(CN)6]^{3-/4-}$ with 1 mol L^{-1} KNO_3: anodic and cathodic peak potentials E_{pa}/E_{pc}, peak potential separation ΔE, anodic and cathodic peak currents I_{pa}/I_{pc}. The charge-transfer resistances R_{ct} obtained from electrochemical impedance spectroscopy measurements are shown for comparison**.**

	E_{pa} (mV)	E_{pc} (mV)	ΔE (mV)	I_{pa} (µA)	I_{pc} (µA)	I_{pa}/I_{pc}	R_{ct} (Ω)
P2	186	110	76	73.65	86.34	0.85	925
P3	186	110	76	111.93	118.35	0.95	850
P4	188	110	78	158.54	164.24	0.97	652
P5	188	110	78	135.62	143.82	0.94	725
P6	168	78	90	64.23	67.30	0.96	980
P7	184	112	72	50.70	63.32	0.80	1210

P5 and **P6** show two oxidation peaks at the anodic peak potentials E_{pa}^{ox} = 1.04/0.83 and 0.93/0.80 eV *vs* Ag/AgCl, respectively, which were ascribed to the formation of radical cation and dication species (**Figure 6** and **Figure S27** in the Supporting Information). The first oxidation of the phenothiazine moiety leads to the formation of a radical cation species at the nitrogen center, which is converted to the dication species by further oxidation of the electron pair at the sulfur atom. Upon scanning in the negative region (-2 and -1.2 V vs Ag/AgCl), all the co-poly-ynes exhibited electron acceptor dependent reduction waves (**Figure S28,** Supporting Information). The measured redox potentials were also used to determine the energy levels of the frontier orbitals (i.e. the HOMO and LUMO) according to:[36]

$$E_{HOMO}/E_{LUMO} = [-(E_{onset} - 0.38) - 4.8] \text{ eV}$$

where the reference energy level of ferrocene is 4.8 eV below the vacuum level and the E_{onset} of the ferrocene/ferrocenium couple vs. Ag/AgCl is 0.38 eV. The calculated HOMO and LUMO levels are presented in **Table 7** and give electrochemical band gaps $E_{g,ele}$ in the range of 1.37-1.77 eV. These are notably smaller than the measured optical band gaps, but this is expected as they refer to distinct processes - the optical bandgaps correspond to the energies required to effect a “vertical” excitation or to form a bound exciton, whereas the electrochemical (transport) band gaps are the energies required to form free carriers.[37, 38]

The redox behavior of the co-poly-ynes suggest that p- and n-type doping of these materials to form conducting states would be feasible, so the systems could be used as electrochemically amphoteric push-pull chromophores that can accept or release electrons at relatively low voltages. They could also be utilized for applications in organic light-emitting diodes (OLEDs) or organic field-effect transistors as functional hole- and electron-transport layers. Additionally, the highly fluorescent co-poly-ynes **P2**-**P3** and **P5**-**P7** could also potentially serve as redox-switchable emitters in OLED devices. We explore some of these points further in the following subsection.

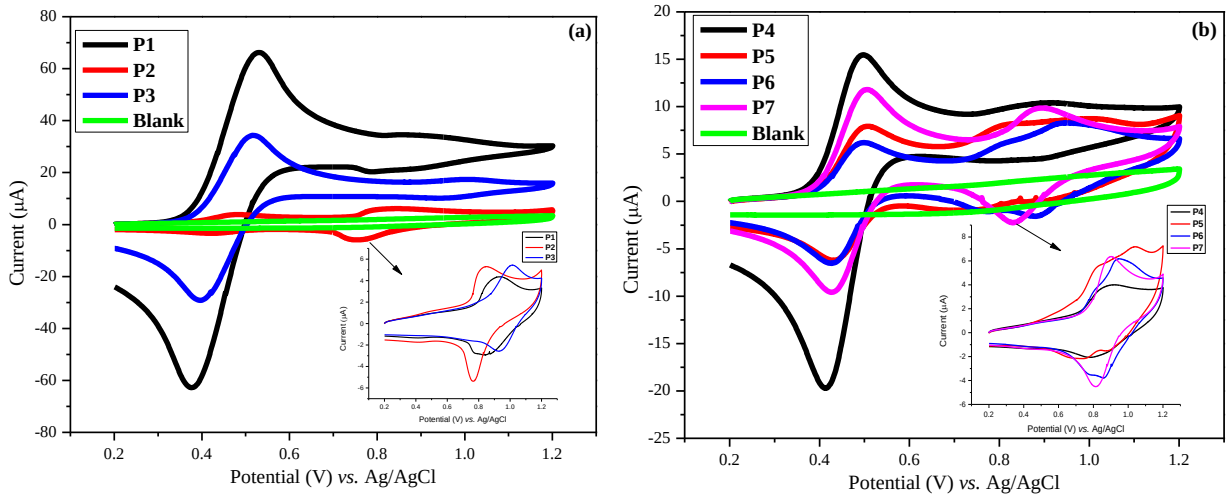

Figure 6 Cyclic voltammograms of polymer-modified interfaces with (a) **P1** – **P3** and (b) **P4** – **P7** in 0.1M Bu_4NPF_6/CH_2Cl_2 solution with ferrocene as a reference, at a scan rate of 100 mV/s, at positive potentials.

Table 7 Electrochemical redox properties of the co-poly-ynes **P1** – **P7** in 0.1M Bu_4NPF_6/CH_2Cl_2 solution using ferrocene as a reference: oxidation and reduction onset and peak potentials $E^{ox}_{onset}/E^{red}_{onset}$ and $E^{ox}_{peak}/E^{red}_{peak}$, HOMO and LUMO energy levels E_{HOMO}/E_{LUMO} and derived electrochemical bandgap $E_{g,ele}$.

	E^{ox}_{onset} (V)	E^{red}_{onset} (V)	E^{ox}_{peak} (V)	E^{red}_{peak} (V)	E_{HOMO} (eV)	E_{LUMO} (eV)	$E_{g,ele}$ (eV)
P1	0.72	-1.05	0.91, -1.10	0.78, -1.18	-5.14	-3.37	1.77
P2	0.72	-0.72	0.83, -0.68	0.94, -0.91	-5.14	-3.70	1.44
P3	0.73	-0.70	1.00, -0.64	0.94, -0.96	-5.15	-3.72	1.43
P4	0.71	-0.72	0.88, -0.69	1.00, -0.91	-5.13	-3.70	1.43
P5	0.71	-0.71	1.04, 0.83, -0.75	0.88, 0.72, -0.93	-5.13	-3.71	1.42
P6	0.69	-0.72	0.93, 0.80, -0.70	0.86, 0.76, -0.95	-5.11	-3.70	1.41
P7	0.72	-0.65	0.89, -0.68	0.88, -0.94	-5.14	-3.77	1.37

2.5. Electroluminescence in polymer light-emitting diodes (PLEDs)

The strong photoluminescence (PL) efficiency of the polymers in solution suggests potential applications in polymer light-emitting diodes (PLEDs).[39-41]

We therefore took **P7** as a base to optimize electroluminescent devices with single emissive layers, comprising stacks of ITO/PEDOT:PSS (40 nm)/TFB (20 nm)/**P7**:PVK (30 nm)/TPBi (20 nm)/LiF (1 nm)/Al (100 nm). (ITO - indium tin oxide; PEDOT:PSS - poly(3,4-ethylenedioxythiophene)/poly(styrenesulfonate); TFB - poly(9,9-dioctylfluorene-co-N-(4-butylphenyl)diphenylamine); PVK - poly(9-vinylcarbazole); TPBi - benzimidazol-2-yl)benzene.) Here, PEDOT:PSS and TFB serve as the hole-injection and hole-transporting materials, respectively, TPBi serves as both an electron-transporting and a hole-blocking material, and LiF serves to enhance the electron injection. The **P7**:PVK layer was spin-coated from a chlorobenzene solution with a controlled ratio and film thickness.

In order to obtain high-performance devices, different doping concentrations of **P7** in the PVK host material were tested. The electroluminescence spectra and current density-voltage-luminance (*J*-*V*-*L*), current efficiency-luminance (CE-*L*), power efficiency-luminance (PE-*L*) and external quantum efficiency-luminance (EQE-*L*) characteristics of the devices are shown in **Figure S29-S32** (Supporting Information). These tests indicated that a 30 nm **P7**:PVK layer containing 10 wt. % of the co-poly-yne exhibited the best performance, with a peak emission wavelength of 518 nm, a maximum current efficiency of 3.34 cd A^{-1}, a maximum power efficiency of 3.16 lm W^{-1}, and a maximum external quantum efficiency (EQE) of 1.21 %. In this device geometry, a brightness of 1.1×10^4 cd m^{-2} was obtained, which is higher than reported for other poly-yne based PLEDs.[42, 43] The results are also comparable to or higher than other reported PTZ-based OLED materials.[41, 44] We also noted a clear emission shoulder between 400-500 nm which decreased in intensity with increasing doping concentration, and which may therefore be emission from the PVK host material.

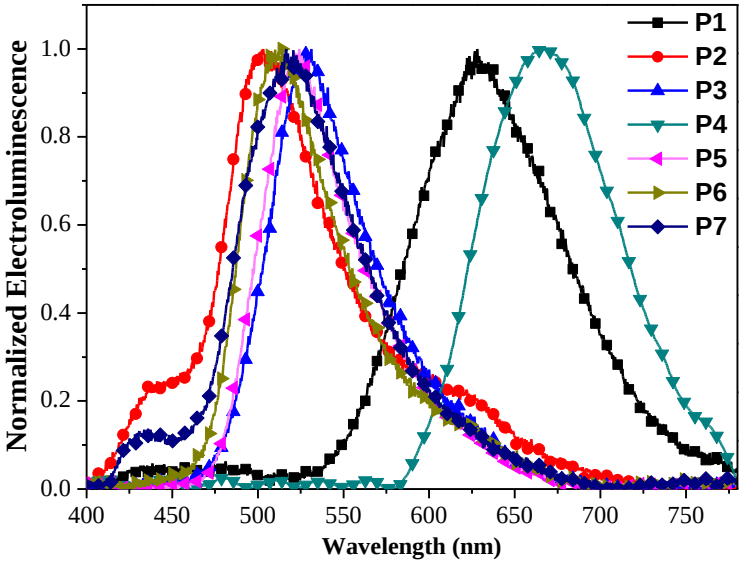

Figure 7 Electroluminescence (EL) emission spectra of polymer light-emitting diode (PLED) devices based on the organic co-poly-ynes **P1** – **P7**.

We next proceeded to fabricate devices based on **P1**-**P6** using the optimal configuration identified for **P7**. Electroluminescent devices based on these polymers exhibited emission ranging from green to deep red and near-infrared (NIR) (**Figure 7**). The *J*-*V*-*L* curves of the devices are compared in **Figure S33** (Supporting Information). The maximum emission wavelengths and corresponding Commission Internationale de L'Eclairage (CIE) coordinates and the turn-on voltages, maximum luminance, current and power efficiencies, and external quantum efficiencies of the devices are compared in **Table 8**. **Figure 8** compares the CE-*L*, PE-*L* and EQE-*L* of the devices based on **P1**, **P3**, **P5**, and **P7**, and the corresponding measurements for devices based on **P2**, **P4**, and **P6** are shown in **Figure S34** (Supporting Information).

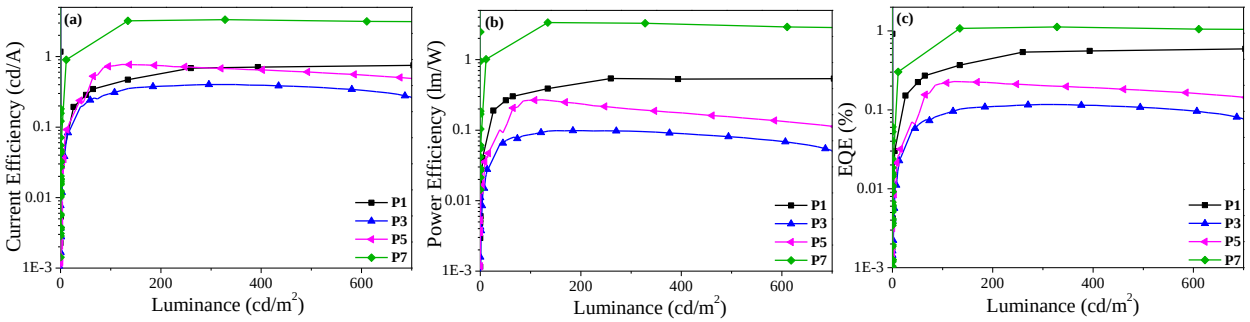

Figure 8 Current efficiency-luminance (CE-*L*) (a), power efficiency-luminance (PE-*L*) (b), and external quantum efficiency-luminance (EQE-*L*) (c) curves for polymer light-emitting diode (PLED) devices based on the organic co-poly-ynes **P1**, **P3**, **P5**, and **P7**.

Table 8 Electroluminescence properties of polymer light-emitting diode (PLED) devices based on the organic co-poly-ynes **P1**-**P7**: peak electroluminescent emission wavelength λ_{EL} and corresponding CIE color coordinates, maximum luminance L_{max}, turn-on voltage V_{on}, maximum current and power efficiency (CE/PE), and maximum external quantum efficiency (EQE).

	λ_{EL} (nm)	CIE	L_{max} (cd m^{-2})	V_{on} (V)	CE (cd A^{-1})	PE (lm W^{-1})	EQE (%)
P1	627	(0.59, 0.37)	3160	2.9	0.79	0.52	0.60
P2	503	(0.26, 0.44)	168	5.0	0.17	0.06	0.07
P3	528	(0.32, 0.60)	700	6.2	0.39	0.10	0.18
P4	667	(0.64, 0.29)	45	7.0	0.03	0.01	0.06
P5	525	(0.31, 0.61)	619	4.8	0.77	0.27	0.22
P6	511	(0.28, 0.57)	539	6.0	0.27	0.08	0.09
P7	518	(0.28, 0.52)	10776	2.7	3.34	3.16	1.21

2.6. Power-conversion efficiency in polymer solar cells

Polymer solar cells (PSCs) using the co-poly-ynes with relatively high absorption coefficients (**P5**/**P7**) and with more red-shifted absorption profiles (**P1**/**P4**) as electron donors and phenyl-C61-butyric acid methyl ester (PCBM) as an electron acceptor were fabricated and characterized (**Table 9**). ITO spin-coated with PEDOT:PSS was used as the hole-collecting electrode, while the electron-collecting electrode was formed from Al/Ca.

Figure 9 shows the *J*-*V* curves of solar cells with 1:1 w/w donor and acceptor active layers under simulated AM1.5 solar irradiation. The power-conversion efficiency (PCE) of the devices increases in the order **P5** < **P4** < **P7** < **P1**. The best-performing cell is that with **P1** as an electron donor, which has an open-circuit voltage (V_{oc}) of 0.46 V, a short-circuit current density (J_{sc}) of 1.94 mA cm^2, and an electrical fill factor (FF) of 27.17 %, resulting in an overall PCE of 0.24 %. This device shows a markedly better J_{sc} and PCE compared to devices based on the other co-poly-ynes in the same blend ratio. Efficient conversion depends on both the absorption wavelength and the absorption coefficient, and the enhanced absorption coefficient of **P1**, obtained by increasing the co-poly-yne conjugation chain length with additional thienyl rings,

suggests this represents an effective strategy for optimizing the co-poly-ynes to improve the PSC performance. The requirement for a high absorption coefficients is also seen in the relative performance of **P5**/**P7** (ε = 13.8 x 10^4/10.2 x 10^4 M^{-1} cm^{-1}) and **P4**/**P1** (10.6 x 10^4/10.0 x 10^4 M^{-1} cm^{-1}).

Table 9 Device characteristics of polymer solar cells made with 1:1 blends of the co-poly-ynes **P1**, **P4**, **P5** and **P7** and PBCM as the donor materials with the specified film thickness: short-circuit current density (J_{sc}), open-circuit voltage (V_{oc}), fill factor (FF), power-conversion efficiency (PCE), and integrated current from external quantum efficiency (EQE). The characteristics of a device using pure PCBM as a donor are shown for comparison.

Donor	Film thickness (nm)	J_{sc} (mA/cm^2)	V_{oc} (mV)	FF (%)	PCE (%)	Integrated current (EQE) (mA/cm^2)
P1	84	1.94	0.46	27.17	0.24	2.09
P4	90	0.56	0.51	25.92	0.07	0.70
P5	110	1.19	0.17	26.08	0.05	1.04
P7	72	0.76	0.43	29.69	0.10	1.18
PCBM	77	0.05	0.003	0	0	-

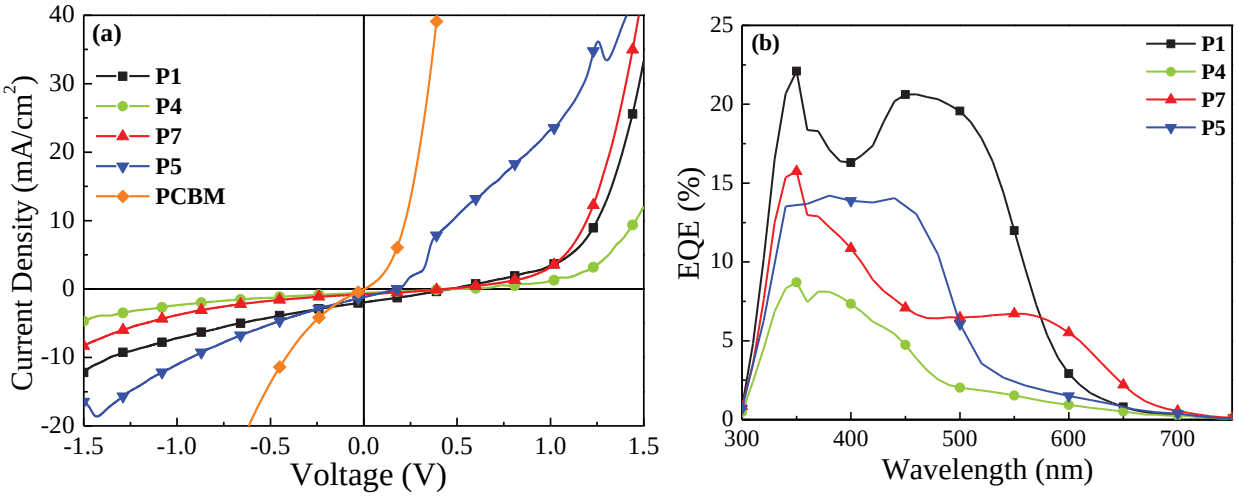

Figure 9 (a) Current density-voltage (*J*-*V*) and (b) external quantum efficiency (EQE) curves for polymer solar cells made with 1:1 blends of the co-poly-ynes **P1**, **P4**, **P5**, **P6** and **P7** and PCBM as donor materials. The *J*-*V* curves also show measurements performed on a device using PCBM as a donor material for comparison.

The best-performing **P1** device was further optimized by varying the spin-coating rate from 600-1800 rpm (**Figure S35**, **Table S11**, Supporting Information), producing film thicknesses from 54-115 nm. We found that a speed of 1200 rpm, which produces a film of *ca*. 84 nm, gave the optimal device characteristics.

The relatively small electrochemical band gaps of **P1**, **P4**, **P5** and **P7** translate to low V_{oc} values of 0.46, 0.51, 0.43 and 0.17 V, respectively. Moreover, the LUMO level of the PCBM acceptor (-3.41 eV)[45] is higher than the electrochemical LUMO levels of **P4** (-3.70 eV), **P5** (-3.71 eV) and **P7** (-3.77 eV), but lower than that of **P1** (-3.37 eV), which explains the low PCE of the devices based on **P4**, **P5** and **P7** (c.f. **Table**

9). The design of polymers for photovoltaic applications should therefore consider the optical bandgap, the absorption coefficient, the absolute positions of the energy levels, and optimizing the thickness of the blend films.

The fill factors are not particularly high in our devices because all processing, save for the PEDOT:PSS annealing and electrode deposition, and all measurements were performed in ambient air, which likely results in the formation of trap states. We therefore expect that the fill factors could be improved by fabricating and characterizing the devices under inert atmosphere. A more comprehensive study of charge transport and the influence of traps is therefore necessary to further improve the overall device performance. Nonetheless, these studies demonstrate that our approach of optimizing the spacer group in PTZ-based co-poly-ynes can potentially serve as a "bottom-up" strategy to designing high-performance PSCs.

3. Conclusions

We have synthesized and characterized a series of seven acetylide-functionalized phenothiazine-based organic co-poly-ynes. The synthetic procedure we presented affords the co-poly-ynes in moderate to high yields of 28-83 %, and the formation of the desired products was confirmed by spectroscopic characterization. GPC indicates molecular weights between 4,000-50,000 g mol^{-1}, corresponding to degrees of polymerization between 13 and 213, and relatively narrow polydispersity indices of 1.12-1.78.

Optical absorption measurements reveal absorption coefficients on the order of 10^5 mol^{-1} cm^{-1} and optical bandgaps in the range of 1.92-2.63 eV. With the exception of **P1** and **P4**, the materials show emission in solution, with quantum yields in the range of 13-41 % relative to Rhodamine 6G. Quantum-chemical calculations on the precursor PTZ moiety **4** and model compounds **M1**-**M7** approximating **P1**-**P7** highlight the role of the spacer group and the extended conjugation in the co-poly-ynes on narrowing the bandgap, pushing the absorption into the visible region of the electromagnetic spectrum and enhancing the absorption coefficient. Electrochemical impedance spectroscopy shows that interfaces modified with **P4** had the lowest charge-transfer resistance of R_{ct} = 652 Ω. The HOMO and LUMO levels were derived from electrochemical measurements of the oxidation and reduction potentials in solution and found to be in the range of -5.11 to -5.15 eV and -3.37 to -3.77 eV, respectively, giving electrochemical band gaps between 1.37-1.77 eV.

Finally, we also assessed the performance of the co-poly-ynes in polymer light-emitting diode (PLED) and bulk heterojunction polymer solar cell (PSC) devices. **P7** exhibited the best PLED performance with a peak emission wavelength of 518 nm, maximum current efficiency of 3.34 cd A^{-1}, maximum power efficiency of 3.16 lm W^{-1}, and maximum external quantum efficiency of 1.21 %. **P1** and **P4**, which did not show emission in solution, were found to show electroluminescent emission at long wavelengths. PSCs fabricated using a 1:1 blend of PCM and **P1** exhibited a moderate power conversion efficiency of 0.24 %, which might be improved by fabricating and testing devices under inert atmosphere. The lower PCEs obtained using donors based on the other co-poly-ynes are likely attributable to the LUMO levels being lower than those of the PCBM acceptor (-3.41 eV).

In summary, we find that the extended conjugation in the co-poly-ynes result in strong absorption and emission in the visible region of the spectrum together with a range of electrochemical properties that make these materials suitable for a range of molecular electronic devices. This is confirmed by the demonstration of working PLED devices with green to deep red and near-infrared emission and a functional PSC device that operates with acceptable power-conversion efficiency, obtained without optimization, based on one of the polymers.

To the best of our knowledge, this is the first report of co-poly-ynes incorporating PTZ as the donor molecule for PLED and PSC devices, and our results not only provide a better understanding of the relationship between the structures of the donor-acceptor systems and their optoelectronic properties, but also highlight a flexible route to designing novel PTZ-based co-poly-ynes for organic electronics. Overall, our results shed valuable light on the relationships between the molecular and electronic structure in this family of materials, demonstrating that the optoelectronic properties can be tuned by careful selection of the spacer group for solid-state lighting and solar-energy harvesting.

4. Experimental Section

4.1. General Procedures

All reactions were conducted under dry Ar using standard Schlenk techniques. Unless stated otherwise, all chemicals were obtained from Sigma-Aldrich and used as received. NMR spectra were recorded in $CDCl_3$ using Bruker WM-250 and AM-400 spectrometers and a Bruker Avance III HD 700 MHz spectrometer equipped with 5 mm TCI H/C/N cryoprobe. The ^{1}H and ^{13}C NMR spectra were referenced to solvent resonances. IR spectra were recorded in attenuated total reflectance (ATR) mode on Diamond using a Cary 630 FT-IR spectrometer. UV/vis spectra were recorded using a Shimadzu UV- 2450 spectrometer. Electrospray ionization (ESI) mass spectra were recorded using a Kratos MS 890 spectrometer. Microanalyses were performed at the Department of Chemistry, Sultan Qaboos University. Preparative thin layer chromatography was carried out on commercial Merck plates with a 0.25 mm silica layer. Column chromatography was performed using Kieselgel 60 silica gel (230−400 mesh).

4.2. Synthesis of PTZ-based ligand

4.2.1.10-(2-Ethylhexyl)-10H-phenothiazine (1)

A reaction mixture of 2-ethylhexyl bromide (16.58 g), phenothiazine (10 g, 0.051 mol) and potassium *t*-butoxide (5.72 g, 0.051 mol) in tetrahydrofuran (THF, 200 ml) was refluxed overnight. After completion of the reaction, removal of the solvent *in vacuo* followed by purification using column chromatography gave the title compound as a colorless viscous liquid (14.28 g, 90%). The resulting liquid was further purified by column chromatography (9.53 g, 67 %). ^{1}H NMR (700 MHz, $CDCl_3$): δ_H/ppm 7.05-7.02 (m, 4H), 6.81-6.77 (m, 4H), 3.61 (d, 2H), 1.84 (m, 1H), 1.37-1.22 (m, 1H), 1.18-1.16 (b, 6H), 0.82-0.75 (m, 6H).^{13}C NMR (176 MHz, $CDCl_3$): δ_C/ppm 145.83, 127.64, 127.17, 125.90, 122.44, 116.00 (aromatic), 51.12 (NCH_2), 35.85 (alkyl CH), 30.82, 28.67, 24.13, 23.17 (alkyl CH_2), 14.13, 10.60 (alkyl CH_3). Anal. calc.

for $C_{20}H_{25}SN$: C – 77.12, H – 8.09; N – 4.50 %; found C – 76.69, H – 8.12, N – 4.48 %. ESI-MS: *m*/*z* 312.3 $[M + 1]^+$.

4.2.2.3,7-Dibromo-10-(2-ethylhexyl)-10H-phenothiazine (2)

To a solution of (*N*-ethylhexylphenothiazine) (5.00 g, 0.016 mol) in DMF (50 mL) was added 2.2 eq. of *N*-bromosuccinimide (17.3 g, 0.97 mol) in portions at room temperature, and the reaction mixture was stirred overnight. After reaction completion, water (100 mL) was added to the reaction mixture followed by saturated aqueous sodium thiosulfate (20 mL), and the organic product was extracted with hexane (2 × 300 mL). The combined organic layer was dried over anhydrous $MgSO_4$. The solvent was removed under reduced pressure yielding a pale-yellow liquid (5.00 g, 69 %). ^{1}H NMR (700 MHz, $CDCl_3$): δ_H/ppm 7.11-7.09 (dd, 2H), 7.06 (d, 2H), 6.54 (d, 2H), 3.51-3.8 (m, 2H), 1.77-1.74 (q, 2H), 1.33-1.22 (m, 6H), 1.19-1.14 (d, 1H), 0.78-0.74 (m, 6H). ^{13}C NMR (176 MHz, $CDCl_3$): δ_C/ppm 144.35, 129.91, 129.65, 127.07, 116.95, 114.64 (aromatic), 51.05 (N−CH_2), 35.69 (alkyl CH), 30.53, 28.44, 23.86, 22.99 (alkyl CH_2), 14.01, 10.44 (alkyl CH_3). Anal. calc. for $C_{20}H_{23}Br_2SN$: C - 43.66, H - 2.88; N - 3.64 %; found C - 43.52, H - 2.88, N - 3.65 %. ESI-MS: *m*/*z* 470.1 $[M + 1]^+$.

4.2.3.3,7-Bis(trimethylsilylethynyl)-*N*-(2-ethylhexyl) 10H-phenothiazine (3)

To a solution of 3,7-dibromo-10-(2-ethylhexyl)-10H-phenothiazine **1** (1.00 g, 2.10 mmol) in ^{i}Pr$_2$NH/THF (70 mL, 1:4 v/v) under an Ar atmosphere was added catalytic amounts of CuI (10 mg), $Pd(OAc)_2$ (10 mg), and PPh_3 (52 mg). The solution was stirred for 30 min at room temperature, and then trimethylsilylethyne (0.61 mL, 4.28 mmol) was added under vigorous stirring. The reaction mixture was then refluxed overnight. The completion of the reaction was confirmed by preparative TLC and IR spectroscopy. After being cooled to room temperature, the mixture was filtered and concentrated under reduced pressure. The crude residue was dissolved in CH_2Cl_2 and purified by silica column chromatography using a hexane/CH_2Cl_2 (1:1 v/v) eluent to yield a yellowish viscous liquid (0.79 g, 75 %) IR (ATR, diamond): *v*/cm^{-1} 2151 (C≡C). ^{1}H NMR (700 MHz, $CDCl_3$): δ_H/ppm 7.17-7.15 (m, 4H), 7.07 (s, 2H), 3.43-3.39 (m, 2H, NCH_2), 1.66-1.62 (q, 2H), 1.20-1.09 (m, 1H), 1.05 (m, 6H, alkyl CH_2), 0.70-0.63 (m, 6H, CH_3), 0.09 (b, 18H, $SiMe_3$). ^{13}C NMR (176 MHz, $CDCl_3$): δ_C/ppm 145.16, 130.99, 130.53, 124.95, 117.21, 115.63 (aromatic), 104.42, 93.77 (C≡C), 50.93 (NCH_2), 35.70 (alkyl CH), 31.73, 28.70, 23.30, 22.97 (alkyl CH_2), 13.86, 10.40 (alkyl CH_3), 0.0 ($SiMe_3$). ESI-MS: *m*/*z* 503.3 (M^+). Anal. calc. for $C_{30}H_{41}NSSi_2$: C - 71.51, H - 8.20, N - 2.78 %; found: C - 71.48, H - 8.19, N - 2.75 %.

4.2.4.10-(2-Ethylhexyl)-3,7-diethynyl-10H-phenothiazine (4)

Bis(trimethylsilylethynyl) product **3** (0.60 g, 1.20 mmol) was proto-desilylated in THF/methanol (20 mL, 4:1, v/v) using aqueous KOH (0.13 g, 2.40 mmol). The reaction mixture was stirred at room temperature for 1 h, during which time preparative TLC and IR revealed that all the protected compound had been converted to the terminal alkyne ligand. The solvent was then removed, and the residue was dissolved in CH_2Cl_2 and purified by column chromatography on silica using hexane/CH_2Cl_2 (1:1, v/v) as eluent, to give the product as a yellow liquid (0.431 g, 100 %). IR (ATR, diamond): *v*/cm^{-1} 2104 (C≡C), 3276 (C≡C-H).^{1}H

NMR (700 MHz, $CDCl_3$): δ_H/ppm 7.21-7.20 (dd, 2H), 7.17 (s, 2H), 6.71 (d, 2H), 3.66-3.60 (m, 2H, NCH_2), 2.97 (s, 2H, C-H), 1.38-1.25 (m, 1H), 1.17 (b, 8H, alkyl CH_2), 0.79-0.77 (t, 6H, CH_3), ^{13}C NMR (176 MHz, $CDCl_3$): δ_C/ppm 145.67, 131.38, 130.98, 125.22, 116.33, 115.73 (aromatic), 82.91 (C≡C), 51.17 (NCH_2), 35.87 (alkyl CH), 30.56, 28.49, 23.89, 23.01 (alkyl CH_2), 14.20, 10.43 (alkyl CH_3). ESI-MS: *m*/*z* 359.2 (M^+). Anal. calc. for $C_{24}H_{25}NS$: C - 80.18, H - 7.01, N - 8.92 %; found: C - 80.20, H - 6.99, N - 8.90 %.

4.3. Synthesis of PTZ-based co-poly-ynes

4.3.1.Co-poly-yne P1

To a stirred mixture of **4** (0.150 g, 0.42 mmol) and 4,7-dibromo2,1,3-benzothiadiazole (0.13 g, 0.42 mmol) in $^{i}Pr_2NH$ (20 mL) and CH_2Cl_2 (20 mL) was added CuI (1 mg). The solution was stirred at room temperature under Ar over a period of 18 h, after which all volatile components were removed under reduced pressure. The crude product was dissolved in CH_2Cl_2 and passed through a silica column using hexane/CH_2Cl_2 (1:1, v/v) as the eluent. The solvent mixture was removed under reduced pressure and the concentrated solution was added to methanol with vigorous stirring to precipitate a red solid (76.6 %). IR (ATR, diamond): *v*/cm^{-1} 2087 (C≡C). ^{1}H NMR (700 MHz, $CDCl_3$): δ_H/ppm 7.76 (b, 2H, BTD_H), 7.50-7.44 (m, 4H, PTZ_H), 6.90 (s, 2H, PTZ_H), 3.80-3.77 (dd, 2H, NCH_2), 2.19 (s, 1H, CH), 1.59 (d, 2H, CH_2) 1.30-1.27 (m, 6H, CH_2), 0.92-0.89 (b, 6H, CH_3). ^{13}C NMR (176 MHz, $CDCl_3$): δ_C/ppm 154.37, 145.82, 132.45, 132.14, 131.38, 130.79 (aromatic), 97.05, 85.78 (C≡C), 51.35 (NCH_2), 36.01 (alkyl CH), 30.95, 28.51, 23.93, 23.01 (alkyl CH_2), 14.02, 10.50 (alkyl CH_3). Anal. calc. for $C_{28}H_{25}N_3S_2$: C - 71.61, H - 5.79, N - 8.95 %; found: C - 71.60, H - 5.65, N - 8.91 %. M_w (g mol^{-1}): 50,100, M_n: 44,600, PDI: 1.12. Decomposition temp.: 170 °C.

4.3.2.Co-poly-yne P2

A similar procedure used to synthesize **P1** was followed using **4** and 2,5-dibromothieno[3,2-b]thiophene to obtain a yellow solid (28%). IR (ATR, diamond): *v*/cm^{-1} 2093 (C≡C). ^{1}H NMR (700 MHz, $CDCl_3$): δ_H/ppm 7.3 (m,7H), 6.80-6.78 (d, 1H, PTZ_H), 3.51- 3.48 (b, 2H, NCH_2), 2.17 (s, 1H, CH), 1.55 (s, 2H, CH_2), 1.25 (b, 6H, CH_2), 0.86 (b, 6H, CH_3). ^{13}C NMR (176 MHz, $CDCl_3$): δ_C/ppm 144.43, 136.04, 131.84, 130.53, 129.74, 129.23, 128.59, 124.28, 115.82, 114.86 (aromatic), 93.24, 92.43, 81.46, 80.48 (C≡C), 47.98 (NCH_2), 34.91 (alkyl CH), 30.95, 28.47, 23.01, 19.27 (alkyl CH_2), 14.00, 10.44 (alkyl CH_3). Anal. calc. for $C_{28}H_{27}NS_3$: C - 70.99, H - 5.75, N - 2.96 %; observed: C - 70.92, H - 7.74, N - 2.94 %. M_w (g mol^{-1}): 6,000, M_n: 4,500, PDI: 1.33. Decomposition temp.: 171 °C.

4.3.3.Co-poly-yne P3

A similar procedure described above for **P1** was followed using **4** and 1,4-dibromo-2,3,5,6-tetrafluorobenzene to obtain a yellow solid (77.5 %). IR (ATR, diamond): *v*/cm^{-1} 2090 (C≡C). ^{1}H NMR (700 MHz, $CDCl_3$): δ_H/ppm 7.40-7.30 (m, 4H, PTZ_H), 6.87-6.80 (s, 2H, PTZ_H), 3.77-3.72 (dd, 2H, NCH_2), 2.17 (s, 1H, CH), 1.57 (s, 2H, CH_2), 1.44-1.37 (m, 6H, CH_2), 0.90-0.80 (b, 6H, CH_3). ^{13}C NMR (176 MHz, $CDCl_3$): δ_C/ppm 146.27, 131.49, 131.22, 130.77, 125.40 (aromatic), 115.99 (C≡C), 51.25 (NCH_2), 35.94 (alkyl CH), 30.95, 30.56, 28.51, 23.01 (alkyl CH_2), 14.00, 10.45 (alkyl CH_3). Anal. calc. for $C_{28}H_{23}F_4NS$: C - 69.55, H -

5.21, N - 2.90 %; found C - 69.51, H - 5.19, N - 2.88 %. M_w (g mol^{-1}): 4,200, M_n: 2,400, PDI: 1.75. Decomposition temp.: 135 °C.

4.3.4.Co-poly-yne P4

A similar procedure used to synthesize **P1** was followed using **4** and 5,7-dibromo-2,3-diphenylthieno[3,4-b]pyrazine to obtain a yellow solid (65 %). IR (ATR, diamond): ν/cm^{-1} 2085 (C≡C). ^{1}H NMR (700 MHz, $CDCl_3$): δ_H/ppm 7.56-7.34 (m, 14H, aromatic), 6.89-6.87 (s, 2H, PTZ_H), 3.79-3.52 (dd, 2H, NCH_2), 2.19 (s, 1H, CH) 1.60 (s, 1H, CH_2), 1.57-1.56 (d, 1H, CH_2), 1.43-1.30 (m, 6H, CH_2), 0.91-0.89 (b, 6H, CH_3). ^{13}C NMR (176 MHz, $CDCl_3$): δ_C/ppm 153.99, 145.62, 142.42, 138.80, 131.13-128.09, 125.27 (aromatic), 115.94 (C≡C), 51.37 (NCH_2), 36.02 (alkyl CH), 30.95, 28.51, 23.02, 19.28 (alkyl CH_2), 14.04, 10.50 (alkyl CH_3). Anal. calc. for $C_{40}H_{33}N_3S_2$: C - 77.26, H - 5.67, N - 6.76 %; found: C - 77.18, H - 5.66, N - 6.74 %. M_w (g mol^{-1}): 3,950, M_n: 2,300, PDI: 1.72. Decomposition temp.: 170 °C.

4.3.5.Co-poly-yne P5

A similar procedure used to synthesize **P1** was followed using **4** and 5,5'-dibromo-2,2'-bithiophene to obtain a yellow solid (57 %). IR (ATR, diamond): ν/cm^{-1} 2098 (C≡C). ^{1}H NMR (700 MHz, $CDCl_3$): δ_H/ppm 7.53-7.27 (b, 4H, BTh_H), 7.15-7.10 (m, 4H, PTZ_H), 7.06-7.05 (d, 1H, PTZ_H), 6.99-6.98 (d, 1H, PTZ_H), 3.73 (s, 2H, NCH_2), 2.16 (s, 1H,CH), 1.55 (s, 2H, CH_2) 1.44-1.26 (m, 6H,CH_2), 0.87-0.86 (b, 6H, CH_3). ^{13}C NMR (176 MHz, $CDCl_3$): δ_C/ppm 156.58, 156.52, 142.78, 139.22, 137.23, 129.59, 129.56, 127.70, 127.24, 124.71, 123.38, 121.13, 115.16 (aromatic), 111.96-111.86 (C≡C), 51.37 (NCH_2), 35.83 (alkyl CH), 30.95, 28.61, 23.14, 22.66 (alkyl CH_2), 14.97, 10.47 (alkyl CH_3). Anal. calc. for $C_{30}H_{27}NS_3$: C- 72.10, H - 5.85, N - 2.80 %; found: C - 71.99, H - 5.83, N - 2.77 %. M_w (g mol^{-1}): 16,900, M_n: 13,800, PDI: 1.22. Decomposition temp.: 133 °C.

4.3.6.Co-poly-yne P6

A similar procedure used to synthesize **P1** was followed using **4** and 4,4'-dibromo-1,1'-biphenyl to obtain a yellow solid (83 %). IR (ATR, diamond): ν/cm^{-1} 2088 (C≡C). ^{1}H NMR (700 MHz, $CDCl_3$): δ_H/ppm 7.58-7.53 (b, 6H, Ph_H), 7.47-7.46 (d, 2H, Ph_H), 7.34-7.30 (m, 4H, PTZ_H), 6.84-6.78 (m, 2H, PTZ_H), 3.72 (b, 2H, NCH_2), 2.17 (s,1H, CH), 1.57 (s, 2H, CH_2), 1.43-1.25 (m, 6H, CH_2), 0.88-0.86 (b, 6H, CH_3). ^{13}C NMR (176 MHz, $CDCl_3$): δ_C/ppm 145.81, 145.03, 139.52, 139.28, 131.98, 131.91, 131.20, 130.46, 128.57, 126.80, 125.30, 125.17, 122.70, 121.90 (aromatic), 116.11-115.82 (C≡C), 51.24 (NCH_2), 35.94 (alkyl CH), 30.53, 28.46, 23.86, 23.00 (alkyl CH_2), 13.99, 10.43 (alkyl CH_3). Anal. calc. for $C_{34}H_{31}NS$: C - 83.73, H - 6.82, N - 2.87 %; found: C - 83.7, H - 6.80, N - 2.84 %. M_w (g mol^{-1}): 20,700, M_n: 13,600, PDI: 1.52. Decomposition temp.: 168 °C.

4.3.7.Co-poly-yne P7

A similar procedure used to synthesize **P1** was followed using **4** and 2,5-dibromothiophene to obtain an orange solid (58 %). IR (ATR, diamond): ν/cm^{-1} 2082 (C≡C). ^{1}H NMR (700 MHz, $CDCl_3$): δ_H/ppm 7.33-7.29 (m, 4H, PTZ_H), 7.16-7.15 (d, 1H, Th), 7.12 (s, 1H, PTZ_H), 6.91-6.90 (d,1H, Th) 6.85-6.83 (m,1H, PTZ_H), 3.76-3.74 (b, 2H, NCH_2), 2.20 (s, 1H, CH), 1.58 (s, 2H, CH_2), 1.46-1.25 (m, 6H, CH_2), 0.90-0.88 (b, 6H,

CH_3). ^{13}C NMR (176 MHz, $CDCl_3$): δ_C/ppm 144.43, 136.04, 131.84, 130.53, 129.74, 129.23, 128.59, 124.28, 115.82, 114.86 (aromatic), 93.24, 92.43, 81.46, 80.48 (C≡C), 50.22 (NCH_2), 34.91 (alkyl CH), 29.53, 27.47, 22.88, 21.98 (alkyl CH_2), 12.98, 9.44 (alkyl CH_3). Anal. calc. for $C_{26}H_{25}NS_2$: C - 74.78, H - 6.52, N - 3.35 %; found: C - 74.71, H - 6.50, N - 3.31 %. M_w (g mol^{-1}): 6,000, M_n: 4,650, PDI: 1.29. Decomposition temp.: 121 °C.

4.4. Gel-permeation chromatography

Gel permeation chromatography (GPC) was used to characterize the organic poly-ynes. A Viscotek VE2001 GPCmax instrument equipped with a TDA 305 triple detector array was used, which measures refractive index (RI), light scattering both at right angles and low angles (RALS and LALS respectively) and viscosity. A Viscotek 2600 UV detector was also used. Three Polyanalytik SupeRes™ Series 300 mm × 8 mm linear mixed bed columns with linear polystyrene molar mass ranges of 103 to 106 were used for the analysis. The instrument was operated at 35 °C with a THF flow rate of 1 mL min^{-1}. The absolute number-average molecular weight (M_n), weight-average molecular weight (M_w) and polydispersity index (M_w/M_n) of the synthesized polymers were obtained by analyzing the chromatograms with the OmniSEC 4.6.1 software. An estimated value of 0.12 for the refractive index increment (d*n*/d*c*) was used in all cases.

4.5. Computational modelling

Molecular quantum-chemical calculations were carried out on the precursor PTZ core **4** and seven finite-chain model compounds **M1**-**M7**, approximating **P1**-**P7**, each consisting of a chain of three PTZ and two spacer moieties with the terminal alkyne groups capped by methyl substituents. The calculations were performed in the gas phase using the density-functional theory (DFT) formalism implemented in the Gaussian09 software.[46] The calculations used the CAM-B3LYP hybrid functional[47]

in conjunction with Pople split-valence basis sets[48] of 6-31g and 6-31g** quality for the H and non-H atoms, respectively. Electronic minimization was performed to tolerances of 10^{-6} and 10^{-8} a.u. on the maximum and root-mean-square (RMS) changes in the density matrix, respectively. Geometry optimizations were performed to tolerances of 4.5×10^{-4} and 3×10^{-4} a.u. on the maximum and RMS force and 1.8×10^{-3} and 1.2×10^{-3} a.u. on the maximum and RMS displacements, and the optimized structures were confirmed to be stationary points on the potential-energy surface by the absence of negative eigenvalues in the nuclear hessian matrices. Time-dependent DFT (TD-DFT) calculations[49] were performed on the optimized structures to identify the lowest-lying 50 (PTZ) or 150 (**M1**-**M7**) singlet and triplet states, and selected states were characterized using the method of natural transition orbitals (NTOs).[30] Visualization of the structures, frontier orbitals and NTOs was performed using the VESTA software.[50]

4.6. Electrochemistry measurements

Electrochemical impedance spectroscopy (EIS) and cyclic voltammetry (CV) measurements were performed on polymer-modified interfaces fabricated by drop casting 5 µL of 1.0 mg L^{-1} stock THF solutions of each of the polymers onto glassy carbon electrodes (GCEs).

To investigate the electrochemical properties of the modified interfaces, these polymer-modified GCEs were used as the working electrode together with platinum wire (Pt) counter and Ag/AgCl (saturated KCl) reference electrodes. EIS measurements were performed over a frequency range from 0.1 Hz to 100 kHz at an amplitude of 5 mV on aqueous solutions of 1.0 mol L^{-1} KNO_3 containing 10^{-2} mol L^{-1} of the $[Fe(CN)_6]^{3-/4-}$ redox system. CV measurements were performed on the same solutions by scanning the potential between -0.2 and 0.6 V at 50 mV s^{-1}. Both sets of measurements were performed at room temperature using a potentiostat interface 1000E (Gamry Instruments).

A further set of CV measurements were carried out on the polymer modified GCEs in 0.1M Bu_4NPF_6/CH_2Cl_2 solution. For these measurements a standard three-electrode configuration employing a Pt wire counter electrode, the modified GCE working electrode, and an Ag/AgCl non-aqueous reference electrode kit was used (BASi, USA). The Ag/AgCl non-aqueous reference electrode was filled with 0.1 M *n*-Bu_4NPF_6 containing *ca*. 10 mM AgCl to provide a constant reference potential; this was subsequently corrected to the ferrocene/ferrocenium potential in the same electrolyte on the day of use. Measurements were performed at a 100 mV s^{-1} scan rate at room temperature using a PalmSens3 computer-controlled potentiostat with the PSTrace electrochemistry software (PalmSens BV).

4.7. Polymer light-emitting diode device fabrication and characterization

Device structures consisting of ITO/PEDOT:PSS (40 nm)/TFB (20 nm)/Polymer:PVK (30 nm)/TPBi (20 nm)/LiF (1 nm)/Al (100 nm) were fabricated to assess the performance of the co-poly-ynes as PLED emitters. (ITO - indium tin oxide; PEDOT:PSS - poly(3,4-ethylenedioxythiophene)/ poly(styrenesulfonate); TFB - poly(9,9-dioctylfluorene-co-N-(4-butylphenyl)diphenylamine); PVK - poly(9-vinylcarbazole); TPBi - benzimidazol-2-yl)benzene.) PEDOT:PSS was deposited on the ITO by spin-coating at 3000 rpm under an N_2 atmosphere, and the TFB layer was then deposited by spin-coating under the same conditions. Room-temperature solutions of the co-poly-ynes in chlorobenzene were prepared (**P1**/**P3**/**P5**-**P7** - 10 mg mL^{-1}, **P2**/**P4** - 5 mg mL^{-1}) and an emissive layer consisting of the polymers in PVK was deposited by spin-coating at 2000 rpm under N_2. Concentrations of 5, 10, 15 and 20 wt. % **P7** and 10 wt. % **P1**-**P6** in PVK were tested. Finally, a 20 nm TPBi layer, a 1 nm LiF cathode and a 100 nm Al capping layer were deposited on top of the emissive layer through a shadow mask under vacuum (2×10^{-4} Pa). The active area of the devices was 2 mm × 2 mm. The electroluninescence spectra of the devices were measured using an Ocean Optics USB 2000 fiber-optic spectrometer in the normal direction. The *J-V-L* curves were measured using a dual-channel Keithley 2614B source measure unit and a PIN-25D silicon photodiode. All measurements were conducted at room temperature under ambient conditions.

4.8. Polymer solar-cell device fabrication and characterization

Device stacks consisting of ITO/PEDOT:PSS (35 nm)/Polymer:PCBM (70-110 nm)/Ca (20 nm)/Al (80 nm) were fabricated to assess the photovoltaic performance of the co-poly-ynes in bulk heterojunction polymer solar cells. (ITO - indium tin oxide; PEDOT:PSS - poly(3,4-ethylenedioxythiophene)/poly(styrenesulfonate); PCBM - phenyl-C61-butyric acid methyl ester.) [TODO]

The active layers were deposited by spin-coating from a 1:1 blend solution (o-dichlorobenzene) of the co-poly-ynes with PCBM with a total concentration of 20 mg mL^{-1} at 800-1800 rpm for 60 s, resulting in films with nominal thicknesses of 70-110 nm as determined using a surface profiler (Alfa Step 500, Tencor). After spin-coating, the samples were transferred to an evaporator and the 20 nm Ca and 80 nm Al layers were thermally deposited under vacuum at 10^{-6} torr to form the top anode. The current-voltage characteristics of the devices were measured using a Keithley 236 source meter under AM 1.5G illumination at 100 mW cm^{-2} produced by a 91160A-1000 solar simulator (Oriel). The external quantum efficiency was measured at a chopping frequency of 275 Hz using a SR830 lock-in amplifier (Stanford Research) under monochromatic illumination from a xenon lamp.

CRediT

Idris Juma Al-Busaidi: Synthesis, Characterization, Investigation, Methodology; **Ashanul Haque:** Funding acquisition, Conceptualization, Investigation, Methodology, Writing - original draft; **Rayya Al-Balushi**: Data curation, Formal analysis; **Jahangir Ahmad Rather:** Data curation, Formal analysis; **Abdul Munam**: Data curation, Formal analysis; **Rashid Ilmi**: Data curation, analysis; **Paul R. Raithby**: Funding acquisition, Writing - review & editing; **Youming Zhang:** Data curation, Formal analysis; **Wai-Yeung Wong**: Funding acquisition, Writing - review & editing; **Jonathan M. Skelton:** Funding acquisition, Investigation, Methodology, Writing - original draft, Writing - review & editing; **Yingying Fu**: Data curation, Formal analysis; **Zhiyuan Xie**: Data curation, Formal analysis; **Shuming Chen**: Data curation, Formal analysis; **Shahidul M Islam**: Data curation, Formal analysis; **Muhammad S. Khan**: Funding acquisition, Conceptualization, Writing - review & editing.

Conflict of Interest

The authors declare no competing financial interests.

ACKNOWLEDGEMENTS

AH extends his appreciation to the Deputy for Research & Innovation, Ministry of Education, Saudi Arabia for funding (project number RDO-2001). MSK thanks the British Petroleum, Oman (Grant EG/SQU-BP/CHI/CHEM/19/01) and the Ministry of Higher Education, Research and Innovation (MoHERI), Oman (Grant RC/RG-SCI/CHEM/20/01) for financial support. IJAB acknowledges the MoHE, Oman for a Ph.D. scholarship. W-YW acknowledges financial support from the Hong Kong Research Grants Council (PolyU 153051/17P), the Hong Kong Polytechnic University (1- ZE1C), Research Institute for Smart Energy (RISE), Ms. Clarea Au for the Endowed Professorship (847S) and the Open Research Fund of State Key Laboratory of Polymer Physics and Chemistry, Changchun Institute of Applied Chemistry, Chinese Academy of Sciences. JMS is currently supported by a UK Research and Innovation Future Leaders Fellowship (MR/T043121/1), and previously held a Presidential Fellowship from the University of Manchester, UK. PRR is grateful to the Engineering and Physical Sciences Research Council (EPSRC) (UK) for continued support (Grant EP/K004956/1).

References

1. C.-L. Ho, Z.-Q. Yu and W.-Y. Wong, *Chem. Soc. Rev.*, 2016, **45**, 5264.
2. A. Haque, R. A. Al-Balushi, I. J. Al-Busaidi, M. S. Khan and P. R. Raithby, *Chem. Rev.*, 2018, **118**, 8474.
3. A. Haque, L. Xu, R. A. Al-Balushi, M. K. Al-Suti, R. Ilmi, Z. Guo, M. S. Khan, W.-Y. Wong and P. R. Raithby, *Chem. Soc. Rev.*, 2019, **48**, 5547.
4. A. Köhler, H. Wittmann, R. Friend, M. Khan and J. Lewis, *Synth. Met.*, 1994, **67**, 245.
5. A. Haque, R. Al-Balushi, I.J. Al-Busaidi, N.K. Al-Rasbi, S. Al-Bahri, M.K. Al-Suti, M.S. Khan, O.K. Abou-Zied, J.M. Skelton, P.R. Raithby, *Inorg. Chem.*, 2021, **60**, 745.
6. (a) I.J. Al-Busaidi, R. Ilmi, J.D.L. Dutra, W.F. Oliveira, A. Haque, N.K. Al Rasbi, F. Marken, P.R. Raithby, M.S. Khan, *Dalton Trans.*, 2021, **50**, 1465; (b) I.J. Al-Busaidi, A. Haque, J. Husband, N.K. Al Rasbi, O.K. Abou-Zied, R. Al Balushi, M.S. Khan, P.R. Raithby, Dalton Transactions, 2021, **50**, 2555.
7. L. Wang, L. Yin, L. Wang, B. Xie, C. Ji and Y. Li, *Dyes and Pigments*, 2017, **140**, 203.
8. R. Grisorio, G. Allegretta, G. P. Suranna, P. Mastrorilli, A. Loiudice, A. Rizzo, M. Mazzeo and G. Gigli, *J. Mater. Chem.*, 2012, **22**, 19752.
9. M. Sailer, M. Nonnenmacher, T. Oeser and T. J. Müller, *Eur. J. Org. Chem.*, 2006, **2006**, 423.
10. M. Sailer, A. W. Franz and T. J. Müller, *Chemistry–A European Journal*, 2008, **14**, 2602.
11. Y. Hua, S. Chang, D. Huang, X. Zhou, X. Zhu, J. Zhao, T. Chen, W.-Y. Wong and W.-K. Wong, *Chem. Mater.*, 2013, **25**, 2146.
12. Y. Hua, S. Chang, H. Wang, D. Huang, J. Zhao, T. Chen, W.-Y. Wong, W.-K. Wong and X. Zhu, *J. Power Sources*, 2013, **243**, 253.
13. Y. Hua, L. T. L. Lee, C. Zhang, J. Zhao, T. Chen, W.-Y. Wong, W.-K. Wong and X. Zhu, *Journal of Materials Chemistry A*, 2015, **3**, 13848.
14. W.-Y. Wong, W.-C. Chow, K.-Y. Cheung, M.-K. Fung, A. B. Djurišić and W.-K. Chan, *J. Organomet. Chem.*, 2009, **694**, 2717.
15. C. H. Siu, L. T. L. Lee, S. C. Yiu, P. Y. Ho, P. Zhou, C. L. Ho, T. Chen, J. Liu, K. Han and W. Y. Wong, *Chemistry–A European Journal*, 2016, **22**, 3750.
16. H. Tian, X. Yang, R. Chen, Y. Pan, L. Li, A. Hagfeldt and L. Sun, *Chemical Communications*, 2007, DOI: 10.1039/B707485A, 3741.
17. W. Wu, J. Yang, J. Hua, J. Tang, L. Zhang, Y. Long and H. Tian, *Journal of Materials Chemistry*, 2010, **20**, 1772.
18. I. J. Al-Busaidi, A. Haque, N. K. Al Rasbi and M. S. Khan, *Synth. Met.*, 2019, **257**, 116189.
19. R. A. Al-Balushi, A. Haque, M. Jayapal, M. K. Al-Suti, J. Husband, M. S. Khan, O. F. Koentjoro, K. C. Molloy, J. M. Skelton and P. R. Raithby, *Inorg. Chem.*, 2016, **55**, 6465.
20. S. Ergun, C. F. Elliott, A. P. Kaur, S. R. Parkin and S. A. Odom, *Chemical Communications*, 2014, **50**, 5339.
21. D. Shinde, J. K. Salunke, N. R. Candeias, F. Tinti, M. Gazzano, P. Wadgaonkar, A. Priimagi, N. Camaioni and P. Vivo, *Scientific reports*, 2017, **7**, 1.
22. A. Köhler, M. Younus, M. R. A. Al-Mandhary, P. R. Raithby, M. S. Khan and R. H. Friend, *Synth. Met.*, 1999, **101**, 246.
23. J. S. Wilson, A. Köhler, R. H. Friend, M. K. Al-Suti, M. R. A. Al-Mandhary, M. S. Khan and P. R. Raithby, *J. Chem. Phys.*, 2000, **113**, 7627.
24. A. Köhler, J. S. Wilson, R. H. Friend, M. K. Al-Suti, M. S. Khan, A. Gerhard and H. Bässler, *The Journal of Chemical Physics*, 2002, **116**, 9457.
25. M. S. Khan, M. K. Al-Suti, M. R. A. Al-Mandhary, B. Ahrens, J. K. Bjernemose, M. F. Mahon, L. Male, P. R. Raithby, R. H. Friend, A. Köhler and J. S. Wilson, *Dalton Trans.*, 2003, **0**, 65.
26. L. Sudha Devi, M. K. Al-Suti, N. Zhang, S. J. Teat, L. Male, H. A. Sparkes, P. R. Raithby, M. S. Khan and A. Köhler, *Macromolecules*, 2009, **42**, 1131.
27. D.-H. Hwang, S.-K. Kim, M.-J. Park, J.-H. Lee, B.-W. Koo, I.-N. Kang, S.-H. Kim and T. Zyung, *Chemistry of Materials*, 2004, **16**, 1298.
28. K. D. Thériault and T. C. Sutherland, *PCCP*, 2014, **16**, 12266.
29. J. M. Skelton, D. S. Gunn, S. Metz and S. C. Parker, *Journal of chemical theory and computation*, 2020, **16**, 3543.
30. M. Frisch, *J. Chem. Phys*, 2003, **118**, 4775.
31. B.-Y. Chang and S.-M. Park, *Annu. Rev. Anal. Chem.*, 2010, **3**, 207.

32. L. Sudha Devi, M. K. Al-Suti, N. Zhang, S. J. Teat, L. Male, H. A. Sparkes, P. R. Raithby, M. S. Khan and A. Köhler, *Macromolecules*, 2009, **42**, 1131.
33. C. S. Krämer, K. Zeitler and T. J. J. Müller, *Tetrahedron Letters*, 2001, **42**, 8619.
34. G. Kim, H. R. Yeom, S. Cho, J. H. Seo, J. Y. Kim and C. Yang, *Macromolecules*, 2012, **45**, 1847.
35. X. Kong, A. P. Kulkarni and S. A. Jenekhe, *Macromolecules*, 2003, **36**, 8992.
36. K.-C. Li, Y.-C. Hsu, J.-T. S. Lin, C.-C. Yang, K.-H. Wei and H.-C. Lin, *Journal of Polymer Science Part A: Polymer Chemistry*, 2009, **47**, 2073.
37. Y. Takeda, T. L. Andrew, J. M. Lobez, A. J. Mork and T. M. Swager, *Angewandte Chemie*, 2012, **124**, 9176.
38. A. Bejan, S. Shova, M.-D. Damaceanu, B. C. Simionescu and L. Marin, *Crystal Growth & Design*, 2016, **16**, 3716.
39. A. Tsuboyama, H. Iwawaki, M. Furugori, T. Mukaide, J. Kamatani, S. Igawa, T. Moriyama, S. Miura, T. Takiguchi, S. Okada, M. Hoshino and K. Ueno, *Journal of the American Chemical Society*, 2003, **125**, 12971.
40. C. W. Tang and S. A. VanSlyke, *Applied Physics Letters*, 1987, **51**, 913.
41. J. Shi, L. Xu, C. Chen, X. Lv, Q. Ding, W. Li, S. Xue and W. Yang, *Dyes and Pigments*, 2019, **160**, 962.
42. C. Schmitz, P. Pösch, M. Thelakkat, H.-W. Schmidt, A. Montali, K. Feldman, P. Smith and C. Weder, *Advanced Functional Materials*, 2001, **11**, 41.
43. E. Smarsly, D. Daume, F. Braig, S. Koser, E. Dörsam and U. H. F. Bunz, *Journal of Materials Chemistry C*, 2018, **6**, 11002.
44. J. Shi, L. Xu, X. Lv, Q. Ding, W. Li, Q. Sun, S. Xue and W. Yang, *Dyes and Pigments*, 2019, **161**, 97.
45. M. Jayapal, A. Haque, I. J. Al-Busaidi, R. Al-Balushi, M. K. Al-Suti, S. M. Islam, M. S. Khan and J. J. Dittmer, *Curr. Org. Chem.*, 2017, **21**, 2017.
46. M. Frisch, G. Trucks, H. Schlegel, G. Scuseria, M. Robb, J. Cheeseman, G. Scalmani, V. Barone, B. Mennucci and G. Petersson, *Journal*, 2009.
47. C. Bannwarth and S. Grimme, *Computational and Theoretical Chemistry*, 2014, **1040**, 45.
48. M. J. Frisch, J. A. Pople and J. S. Binkley, *The Journal of chemical physics*, 1984, **80**, 3265.
49. R. Scuseriaa, *J. Chem. Phys*, 1998, **109**, 8218.
50. J. Laugier and B. Bochu, *Journal*, 2011.